Volume 1 | Number 1 | Jan 2013 | Pages 1–100

Environmental Science
Nano

www.rsc.org/es-nano

ROYAL SOCIETY
OF CHEMISTRY

ROYAL SOCIETY
OF CHEMISTRY

rsc.li/es-nano

Nano Impact Statement

With increased graphene use in consumer products there is a growing concern over its effect on human health and the environment. Quantification methods are needed to understand the risk associated with graphene. In this study, we describe a method for quantifying graphene in complex organic matrices. This method is useful for monitoring graphene in the environment and determining its impact on human health. Given graphene's likelihood to end up in wastewater treatment plants, we demonstrate the applicability of this method for wastewater biosolids. The results presented in this study will also be fundamental for the further development of methods for quantifying graphene in other complex matrices (e.g., sediment, tissue).

1   Quantification of Graphene and Graphene Oxide in Complex Organic Matrices

2

3

4   Kyle Doudrick[1*], Takayuki Nosaka[2], Pierre Herckes[3], and Paul Westerhoff[4]

5

6   [1]Department of Civil and Environmental Engineering and Earth Sciences, University of Notre

7   Dame, Notre Dame, IN 46556, USA

8   [2]School for Engineering of Matter, Transport and Energy, Arizona State University, Tempe, AZ

9   85287-6106, USA

10   [3]Department of Chemistry and Biochemistry, Arizona State University, Tempe, AZ 85287-1604,

11   USA

12   [4]School of Sustainable Engineering and the Built Environment, Arizona State University,

13   Tempe, AZ 85287-5306, USA

14

15

16   *Corresponding author email: kdoudric@nd.edu

17

24   **Abstract**

25   Interest is growing for graphene as a nanomaterial for electronic and composite

26   applications. Increased production and use of graphene warrants development of strategies to

27   detect and monitor its effect on human health and the environment. A quantification method

28   using programmed thermal analysis (PTA) was developed for few-layer graphene (FLG) and

29   graphene oxide (GO). FLG exhibited strong thermal stability, which allowed for easy detection

30   in matrices consisting of thermally weaker background organic carbon. GO (50% oxygen

31   content) exhibited a weaker thermal stability than FLG, making quantification more challenging

32   in the presence of thermally similar background organic carbon. To resolve this, an *in-situ*

33   reduction method using a reducing agent (sodium borohydride) was developed to remove

34   surface-bound oxygen from GO. This was used in combination with a digestate (Solvable^{TM}) to

35   create an optimized extraction method for recovering FLG and GO from complex organic

36   matrices. FLG and GO will enter sewer systems due to their use by industry and in consumer

37   products. We investigated the applicability of this method for quantifying FLG and GO in

38   wastewater biomass because they are likely to accumulate in wastewater biosolids, as these are

39   commonly the first exposure route for novel materials in the environment. Spiking 20 μg of FLG

40   and GO into a 200 mg dried biomass/L wastewater solution resulted in recoveries of $52 \pm 8\%$

41   and $80 \pm 6\%$, respectively. Results from this study can be applied to the development of

42   extraction methods for graphene from similar complex organic matrices (e.g., lung tissue, *in-*

43   *vitro/in-vivo* studies, algae, daphnia) to support a range of human and ecotoxicological studies.

44

Introduction

With the influx of graphene into the composite and electronic markets there is a growing concern about the risk of graphene to human health and the environment.[1, 2] Currently, the lack of established methods for quantifying graphene and the lack of reported methods for extracting graphene from complex matrices limits the ability to conduct appropriate human and eco-toxicity studies. The availability of quantification methods is important for developing reliable dose-response toxicity metrics and for monitoring workplace safety. In the environment, the same quantification methods are useful for determining exposure concentrations and assessing graphene fate and transport routes.

Detection methods such as X-ray diffraction[3] and Raman spectroscopy[4] are useful for characterizing graphene, but they do not allow for appropriate quantitative analysis. Thermogravimetric analysis (TGA) and ultraviolet-visible (UV-Vis) spectroscopy can also be used to detect graphene; they are quantitative methods, although limited in that respect. TGA is useful for determining the thermal stability of graphene and can also quantify purity (i.e., metal content),[5] but it is limited to purer, dry samples rather than graphene in complex environmental or biological matrices. UV-Vis has been used previously to characterize the dispersion state of graphene oxide (GO) in aqueous solutions,[6] and it can be used as a means of quantifying GO in aqueous solutions, but only if the dispersion (i.e., aggregation) state stays constant. The UV-Vis sensitivity becomes poor for graphene (stacked sheets in aqueous matrix) and GO in aqueous solution below approximately 1.5 mg/L and 75 µg/L, respectively (Figure SI-1 showing UV-Vis spectrum for graphene and GO). In more complex matrices (e.g., surface water), quantifying graphene and GO will be more difficult due to different aggregation states and matrix interferences in the same wavelength range, which is especially true for GO (peaks between 220-

3

68   250 nm; Figure SI-1). The lack of analytical methods for quantifying graphene in complex

69   matrices signifies a need to develop robust analytical strategies that include both quantification

70   and sample preparation.

71   We have previously developed a quantification method for carbon nanotubes (CNT),[7] and

72   have applied it to CNTs that were extracted from lung tissue with a high recovery.[8] This

73   quantification method, termed programmed thermal analysis (PTA), is an organic

74   carbon/elemental carbon analysis that determines carbon mass and separates CNTs from other

75   forms of carbon on the basis of the CNT's thermal stability. This separation is achieved using a

76   time-dependent temperature ramp program; thermally weaker carbon compounds (e.g., tissue,

77   bacteria) evolve early in the program while thermally stronger carbon compounds (e.g., CNT,

78   graphene) evolve later. The ability to separate distinct forms of carbon is important for avoiding

79   background interferences when quantifying carbonaceous nanomaterials in complex matrices

80   containing organic carbon.

81   Before PTA can be used to quantify CNTs in complex organic matrices, CNTs must be

82   extracted to separate them from excess carbonaceous material that could interfere with the

83   analysis. With proper extraction methods in place, CNTs can be concentrated and then quantified

84   using a number of methods (e.g., TGA-mass spectrometry,[9] gel electrophoresis,[10] infrared,[11]

85   radio-labeling,[12] microwave,[13] UV-Vis,[14] and inductively coupled plasma-mass spectrometry[15]).

86   Given the physical and chemical similarities between graphene and CNTs, we hypothesize that

87   the same approach can be used for extracting and quantifying graphene.

88   For PTA, oxygen functional groups on CNTs are problematic because they complicate

89   separation of CNTs from organic carbon during analysis.[7] Graphene is expected to be easily

90   amenable to PTA because of its low oxygen content and consequently high thermal stability.[16]

4

91   Alternatively, GO tends to have a very high oxygen content, with a carbon to oxygen ratio (C:O)

92   on the order of 1:1; thus, its thermal behavior is similar to organic carbon. While the similar

93   thermal behavior is not an issue for samples containing only GO (e.g., pure aqueous GO stock

94   solutions), it interferes with analysis when quantifying GO in matrices containing organic

95   carbon. GO can be transformed to "reduced graphene oxide" (RGO) using chemical reducing

96   agents such as hydrazine[17, 18] or sodium borohydride.[19-23] Removing oxygen makes graphene

97   (oxide) more hydrophobic, which increases its tendency to aggregate and results in a more

98   efficient separation and extraction. The key to any successful approach for environmental and

99   biological samples will be doing this *in-situ* (i.e., in a complex matrix) so that GO can easily be

100   recovered.

101   With the increase in graphene production and the advent of new graphene-containing

102   products, graphene is likely to enter into wastewater treatment plants. Given graphene's

103   similarity to CNTs, it will presumably end up in wastewater effluent or wastewater biosolids

104   (treated sewage sludge containing living/dead microbes and inert solids).[24] Of these exposure

105   routes, biosolids seem to be the most appropriate end-point for graphene and GO.[25-28]

106   The aims of this study were to (1) develop a PTA quantification method for graphene and

107   GO and (2) develop a method for recovering graphene and GO from complex organic matrices.

108   We utilized few-layer graphene (10–20 nm thick) in place of single-layer graphene due to the

109   problem obtaining an aqueous solution of single-layer graphene. Because of the difficulty

110   extracting oxygenated carbonaceous nanomaterials (e.g., GO) from complex matrices, we

111   applied an *in-situ* reduction method to increase hydrophobicity and improve recovery. Given the

112   likelihood of graphene to end up in wastewater biosolids, we demonstrated an extraction and

113   quantification method for wastewater biosolids to assist with fate and transport studies. The

114   results stemming from this research can be leveraged to develop extraction methods for graphene

115   from other biological matrices (e.g., lung tissue, *in-vitro/in-vivo* studies, algae, daphnia).

116

117   **Experimental Methods**

118   *Materials*

119   GO solution was used as received (TW Nano; manufacturer reported characteristics: 0.2

120   wt. %, >90% single layer, 0.5–20 µm in x-y, 1:1.3 C:O ratio, >1,200 m^2/g). Graphene

121   nanoplatelet powder was used as received (Angstron Materials, N006-P; manufacturer reported

122   characteristics: >97% carbon, <1.5% oxygen, <1.5% ash, 10–20 nm thick, <14 µm in x-y

123   direction, 21 m^2/g). Graphene nanoplatelets, or few-layer graphene (FLG), are stacked graphene

124   sheets and are used in place of graphene because pristine (i.e., no oxygen) single-layer graphene

125   in aqueous solution is not achievable. GO and FLG consisted of flake like particles with

126   dimensions similar to each other (Figure SI-2, a and c, respectively). SEM images revealed the

127   presence of rectangular plates, with small (x-y < 1 µm) and large (x-y ~ 5–10 µm) fractions for

128   both GO and FLG. FLG was typically smaller than the maximum size listed by the manufacturer

129   (average x-y from Figure SI-2c was approximately 4 x 2.5 µm).

130   Sodium borohydride (99.99%, Sigma Aldrich, 480886), hydroiodic acid (57% in H_2O,

131   Sigma Aldrich, 210013), and ascorbic acid (reagent grade, Sigma Aldrich, A7506) were used as

132   received. Solvable™ was obtained from Perkin Elmer. Solvable is a tissue solubilizer consisting

133   of sodium hydroxide (≤2.5%), C10-16-alkyldimethyl, N-oxide (2–10%), and C11-15-secondary,

134   ethoxylated alcohol (2.5–10%). Sodium hydroxide (97%, EMD SX0590), Tergitol 15-S-12™

135   (C12-14 secondary ethoxylated alcohol, CAS no. 84133-50-6, Dow Chemical Company), and

136   N,N-dimethyldodecylamine, N-oxide (30% in H_2O, Sigma Aldrich 40236) were obtained to

137   examine the individual components of Solvable. Ultrapure water (18.2–18.3 MΩ-cm) was used

138   for all experiments.

139

140   *Programmed Thermal Analysis*

141   PTA was performed using an organic carbon/elemental carbon analyzer (Sunset

142   Laboratory, Inc., Sunset, Oregon, USA). PTA was used to quantify graphene recovery,

143   determine changes in graphene thermal stability after treatment, and quantify the biomass

144   background carbon after treatment; PTA operation is described in detail elsewhere.[7] Briefly,

145   samples were heated using a graphene-specific temperature ramp program (Table SI-1) in inert

146   conditions (100% He) and then in oxidizing conditions (90% He/10% O_2). The carbon that

147   evolves during analysis is converted to methane and then detected using flame ionization

148   detection (FID). This FID signal is calibrated with internal and external standards that are used to

149   calculate the mass of carbon evolved. The graphene-specific program was designed to remove

150   most of the background organic carbon during the initial inert phase and then transition into the

151   oxidizing phase where the more stable background carbon is removed before evolution of

152   graphene. PTA quantifies only the mass of carbon, so the oxgyen mass is not considered for

153   compounds like GO. The maximum temperature under inert conditions was set at 675°C to avoid

154   loss of oxygenated graphene. Samples were put onto a quartz-fiber filter (QFF; Pall Tissuquartz

155   2500 QAT-UP, 7204) designed for high temperatures (Figure SI-3) and then loaded into the PTA

156   instrument for analysis.

157

158   In-situ *Reduction of Graphene Oxide*

159   An *in-situ* reduction method for GO was developed to overcome the difficulty in

160   recovering hydrophilic carbonaceous nanomaterials from aqueous matrices. For reduction

161   experiments, a specified amount (e.g., 0.4%, 2%) of $NaBH_4$ was added to a mixture of GO

162   solution and water or Solvable. Samples were then placed in a furnace at 60 °C for 2 hrs

163   followed by centrifugal separation at 22,830 × g for 10 min and washed twice with water

164   (additional washing causes poor pellet formation). Final pellets were collected and loaded onto a

165   QFF for either Raman or PTA. Samples requiring a phase-separation were treated with $NaBH_4$

166   for 36 hrs rather than 2 hrs.

167

168   *Extraction from Biomass*

169   Biomass was grown using a laboratory-scale sequencing batch reactor that was seeded

170   using return activated sludge from a local (Mesa, AZ) full-scale wastewater treatment plant.[27]

171   1000 µg dry weight (~78 µL) of concentrated fresh biomass stock (12.8 g/L) was added to 5 mL

172   Solvable to obtain a biomass concentration of 200 mg/L. GO or FLG (~20 µg) was then added.

173   The ratio of carbon to biomass was ~0.02 µg C/µg dried biomass. Samples were placed in a

174   furnace at 60 °C for 24 hrs to digest the biomass. After digesting, $NaBH_4$ was added to begin the

175   *in-situ* reduction process. The treated samples were then centrifuged at 22,830 × g for 10 min.

176   The pellet was twice washed with water followed by centrifuging each time. The final pellets

177   were collected using a pipette and then loaded onto a QFF for PTA. Samples were prepared and

178   analyzed in triplicate.

179   The method detection limit (MDL) for GO or FLG in 1000 µg dried biomass was

180   calculated using a *t*-distribution with 99% confidence (one tail, seven replicates, 5 µg

181 graphene).[29] The 95% lower (LCL) and upper (UCL) confidence intervals were calculated as

182 $0.64 \times$ MDL and $2.20 \times$ MDL, respectively.[29]

183

184 *X-ray Photoelectron Spectroscopy*

185 Surface elemental composition and chemical state were analyzed using X-ray

186 photoelectron spectroscopy (XPS) performed on an ESCALAB 220i-XL (Vacuum Generators,

187 U.S.) with a monochromatic Al K_α source at hv = 1486 eV, a base pressure of 7×10^{-10} mbar,

188 and a spot analysis size of 500 µm. For GO and RGO solutions, powders were obtained by

189 evaporating solutions in aluminum trays. The final dried product was crushed using an agate

190 mortar and pestle. All samples were prepared for XPS by pressing the powder into a disk on

191 clean indium foil. Peak fitting was performed manually using XPS peak analysis software (Casa

192 XPS) on the basis of the theoretical atomic percentages calculated from the wide scan.

193

194 *Raman Spectroscopy*

195 Raman spectroscopy was used to determine the changes in the GO structure resulting

196 from the *in-situ* reduction. Raman was performed on a custom-built confocal instrument in 180°

197 geometry. The sample was excited using a 532-nm laser with 100-mW maximum power, which

198 was controlled using neutral density filters. The data were collected using an Acton 300i

199 spectrograph and a back-thinned Princeton Instruments liquid nitrogen–cooled CCD detector

200 with a spatial resolution <1 µm and spectral resolution of ~1 cm^{-1}. Between 1300 and 1600 cm^{-1},

201 there are two distinct peaks for graphene, called the D-band (1350 cm^{-1}) and the G-band (1580

202 cm^{-1}). The D-band is present because of defects or disorder (e.g., sp^3 bonds) present within the

203 graphene sample and increases in intensity with increasing disorder. The G-band is the graphitic

204 band, and a higher, narrower peak indicates a more ordered graphene (i.e., sp^2 bonds). The

205 average I_D/I_G ratio was calculated from measurements taken at four different points for each

206 sample.

207

208 *Scanning Electron Microscopy*

209   Scanning Electron Microscopy (SEM) was completed using a Nova 200 FIB-SEM from

210 FEI with a field-emission electron gun. SEM imaging was performed at 5 kV and 0.98 to 1.6 nA

211 with dwell time between 0.3 and 3 µs.

212

213 *Ultraviolet-Visible Light Spectroscopy*

214   UV-Vis absorption spectra of GO and FLG were investigated on a Hach DR5000. Serial

215 dilutions were made from 2 g/L stock solutions and ultrapure water. All samples were scanned

216 from 200 to 800 nm. For GO, no absorption occurred above 600 nm (brown color in solution)

217 and it had two peaks at 238 and 300 nm. FLG (black color in solution) absorbed across all

218 wavelengths with excellent calibration correlation ($R^2 > 0.99$) and a broad peak at 227 nm.

219

220 **Results**

221 *Graphene Detection*

222   FLG and GO were quantified using PTA, which relies on separating carbon compounds

223 on the basis of their thermal stability in inert (i.e., He) and combustion atmospheres (i.e., 90%

224 He/10% O_2). Weaker compounds and those with more oxygen will evolve during the inert phase

225 and early in the oxidizing phase. Figure 1 shows the PTA result for 20 µg of FLG and GO (run

226 separately). Instrument detection was reliable with calibration data demonstrating a slope of 1.02

227   and an R^2 of 1.00 for both FLG and GO (Figure SI-4). The majority of FLG evolved at high

228   temperatures during the oxidizing phase, starting around 700 °C and peaking around 900 °C,

229   with the strong thermal stability owing to the low defect density and low oxygen content. A

230   small amount of FLG (~3%) evolved during the inert phase (i.e., where background organic

231   carbon would evolve) and can be attributed to the oxygenated FLG. For GO, the high amount of

232   oxygen resulted in a larger portion evolving during the inert phase (~20%), all of which would

233   be lost in the background of a complex organic sample evolving at the same temperatures.[7]

234   Reducing or removing the oxygenated groups on graphene is key to improving the recovery of

235   GO from complex organic matrices.

236

237   *Improving Detection and Extraction of FLG and GO through Reduction*

238   In order to improve GO detection and recovery, different reducing reagents (e.g., sodium

239   borohydride (NaBH$_4$), ascorbic acid, hydroiodic acid (HI)) were investigated to remove oxygen

240   functionalities from GO. Ascorbic acid and HI were not ideal reagents, resulting in incomplete

241   reduction of GO, the inability to fully aggregate GO, or GO adherence to the plastic vials (See SI

242   for further discussion on failed reagents). NaBH$_4$ emerged as the optimal reagent for GO

243   reduction resulting in an increased thermal stability and hydrophobicity.

244   XPS was used to investigate the C-C and C-O/C=O bond content of GO. Figure 2 shows

245   the XPS analysis for GO in water and GO after treatment with NaBH$_4$ in water (i.e., RGO). Two

246   peaks were present, one at 284 eV, which is attributed to C-C/C=C, and the other at 286–290 eV,

247   which coincides to a number of carbon and oxygen functionalities (mainly C-O and C=O). The

248   C-O/C-C ratio for GO was 1.1:1, which agrees with the manufacturer's carbon to oxygen ratio of

249   1:1. The C-O/C-C ratio for RGO was 5.6:1, an approximate 5-fold decrease in the number of C-

250 O/C=O bonds. GO reduction also shifted the C-O peak to lower binding energies, indicating a

251 change in the type of carbon-oxygen functionalities that remained on the GO. These results

252 provide clear evidence that carbon-oxygen functionalities were removed by $NaBH_4$ treatment.

253 SEM images show that reduction of GO (Figure SI-2a) to RGO (Figure SI-2b) did not

254 significantly alter the particle shape or x-y size (e.g., both large, 5–10 μm, and small (e.g., right

255 side of Figure SI-2b), < 1 μm, sheets were present), and stacked, plate-like structures were

256 formed. Figure 3 shows the PTA thermogram for RGO after treatment with 2% $NaBH_4$ in water.

257 Chemical reduction improved the thermal stability (i.e., peak shift to the right), providing

258 additional evidence that oxygen functionalities were removed.

259 Raman spectroscopy is used to determine the defect density of CNTs and graphene,[4]

260 defined as the ratio between the D-band (1350 cm^{-1}) and G-band (1580 cm^{-1}) (I_D/I_G). The defect

261 density is an indication of the thermal stability[7] and the degree of oxidation.[30] We hypothesized

262 $NaBH_4$ reduction would decrease the defect density and result in an increase in the GO thermal

263 stability due to a decrease in the number of oxygen functionalities. However, Raman results

264 revealed that the I_D/I_G did not change significantly (>5%) after $NaBH_4$ treatment. Although

265 reduction of oxygen functionalities occurred (i.e., XPS and thermal stability results), the

266 chemical reduction treatment did not heal defects. $NaBH_4$ is known to reduce aldehydes and

267 ketones into alcohols, and it is capable of reducing lactone and carbonyl groups to hydroxyl

268 groups on functionalized CNTs.[31] So, in the case of $NaBH_4$ reduction of GO, presumably the GO

269 functionalities are only being reduced as far as C-OH and C-H, and $NaBH_4$ is not able to heal

270 defects through C-C sp^2 bond formation.

271 In water, $NaBH_4$ enabled aggregation of GO, presumably a result of removing

272 oxygenated functional groups, but separation via centrifugation was difficult (i.e., Figure SI-5).

273   In a clean, aqueous matrix (i.e., only water and GO), filtration directly onto a quartz-fiber filter

274   (QFF) is an option for separating the GO (e.g., 10-20 µm X-Y dimensions), but this is not an

275   option for complex matrices because the filter will also collect interfering carbon compounds.

276   For applications involving clean matrices free of carbon interferences, filtration may be an

277   option; though retention using the QFFs, which are designed to function as air filters, may be

278   poor for GO as observed for functionalized CNTs.[7] Furthermore, if a different quantification

279   method (e.g., electrophoresis, UV-Vis) is used, the sample would need to be in a concentrated

280   aqueous or powder form and not adhered to a filter.

281   In a Solvable matrix, which is the reagent used to solubilize organics (e.g., wastewater

282   biomass (this paper), tissue[8]), GO aggregated and formed a very stable, compact pellet upon

283   centrifugation. This is likely due to a combination of a high pH, double-layer compression from

284   increased ionic strength, and the presence of two surfactants, which may cause a cloud-point like

285   effect.[32] The known individual components of Solvable were examined to determine the root of

286   the effect. Both surfactants (10% concentration) alone and in combination caused aggregation

287   while sodium hydroxide was not effective. Upon addition of $NaBH_4$ to the surfactants, samples

288   exhibited severe effervescence due to hydrogen generation, and GO was not easily recovered as

289   it adhered to the vials, overflowed the vials along with the bubbles, or would not centrifuge into

290   a pellet. However, adding sodium hydroxide to the two surfactants (individual or combined)

291   curbed the effervescence. Therefore, the excellent performance of Solvable for extracting

292   graphene can be attributed to a synergistic action of its components rather than a single species.

293   Figure 4 shows the percent recovery of RGO as a function of increasing $NaBH_4$ concentration.

294   Recovery with Solvable alone (i.e., no reducing agent) was $75 \pm 0.5\%$. Adding low

295   concentrations of $NaBH_4$ (e.g., 0.04%) did not show improvement with an average recovery of

296   76 ± 3%. Increasing the $NaBH_4$ concentration to 0.4% resulted in a slightly higher recovery (81

297   ± 3%), but recovery over 90% wasn't achieved until greater than 2% $NaBH_4$ was used (95 ±

298   5%), with a maximum recovery of 97 ± 0.4% observed using 8% $NaBH_4$. The improved physical

299   recovery was attributed to a reduction in oxygen content, resulting in increased aggregation of

300   the graphene particles. Removal of carbon-oxygen bonds shifts the hydrophilic nature of

301   graphene to be more hydrophobic, resulting in improved aggregation during centrifugation.

302   Reduction also decreases the amount graphene that would otherwise be lost in the organic carbon

303   PTA background (i.e., during the inert phase as shown in Figure 1).

304   When using PTA for quantifying graphene, the thermal stability (i.e., peak oxidizing

305   temperature) is important for separating graphene from background organic carbon during

306   analysis. Figure 5 shows PTA mass loss curves under oxidizing conditions for GO using

307   different extraction conditions. Surfactants have been previously shown to reduce the thermal

308   stability of CNTs,[7] and we observed the same effect for GO treated with Solvable, an alkali

309   reagent containing surfactants. Solvable decreased the thermal stability of GO significantly, with

310   an onset approximately 130 s earlier and 50 °C lower. Reduction of GO in water with $NaBH_4$

311   improved the thermal stability (Figure 3), so we hypothesized that this would improve the GO

312   stability after Solvable treatment. Using low concentrations of $NaBH_4$ (e.g., 0.04%) after the

313   Solvable treatment only increased the thermal stability slightly (~20 s), but using a higher

314   concentration of $NaBH_4$ (>2%) returned the thermal stability close to the original (Figure SI-6).

315   The improvement in the thermal stability may account for the improved recovery when using

316   greater than 2% $NaBH_4$ (i.e., Figure 4). To achieve optimal extraction, a combination of Solvable

317   and at least 2% $NaBH_4$ is recommended.

318   *Recovery of GO and FLG from Biomass*

14

319   The ability to quantify GO or FLG in a complex organic matrix such as wastewater

320 biosolids is important for assisting environmental studies. As such, we determined detection

321 limits for GO and FLG in biomass as well as recovery of 20 µg of GO or FLG from 1 mg of

322 clean, dried biomass (200 mg/L). The MDL, LCL, and the UCL for GO in biomass were

323 calculated to be 2.2, 1.4, and 4.9 µg, respectively. The MDL, LCL, and UCL for FLG in biomass

324 were calculated to be 1.5, 0.93, and 3.2 µg, respectively. In comparison, the MDL for GO in a

325 clean aqueous matrix (i.e., ultrapure water only) is 1.7 µg.

326   Without Solvable treatment, FLG and GO detection in biosolids was not possible because

327 the amount of biomass collected in the pellet overwhelmed PTA and resulted in indistinguishable

328 peaks for graphene and biomass. Using the extraction method of Solvable and 2% $NaBH_4$,

329 GO/RGO and FLG (20 µg) recoveries from 1 mg dried biomass (0.02 µg graphene/µg dried

330 biomass) were $80 \pm 6\%$ and $52 \pm 8\%$, respectively. Although FLG is easier than GO/RGO to

331 detect in a complex matrix using PTA because it is more thermally stable, physical separation

332 from the biomass using centrifugation was less efficient, resulting in a lower recovery. We

333 observed that FLG was very stable in Solvable (before and after biomass treatment), with little

334 recovery occurring via centrifugation (<5%). Although FLG is already in a "reduced" form,

335 adding $NaBH_4$ helped to improve the FLG aggregation and extraction. We also examined nitric

336 acid as a digesting agent in place of Solvable to determine if pH or surfactants were an issue.

337 Like Solvable, FLG was more stable in nitric acid (pH < 0) than in ultrapure water (pH = 5.6),

338 likely due to increased surface charge separation, but extraction was worse than with Solvable.

339 This agrees with previous results showing Solvable to be optimal over common agents (e.g.,

340 nitric acid, hydrochloric acid, hydrofluoric acid, etc.) used for extracting CNTs from rat lung

341 tissue.[8]

342   Solvable was efficient at dissolving the biomass, but a small amount of background

343   carbon still remained and interfered with GO/RGO peaks (Figure 6); no interference was

344   observed for FLG. The interference for GO/RGO was consistent across triplicate samples with

345   an average of 2.2 ± 1 µg. When the amount of biomass was increased to 5 mg (1 g biomass/L),

346   GO/RGO peaks were indistinguishable due to the false positive from interfering background

347   carbon that remained after treatment. To improve the extraction for GO/RGO from high

348   concentrations of biomass, we developed a phase-separation method by extending the heating

349   time of the $NaBH_4$ step to 36 hrs. This causes the water and surfactant phases of Solvable to

350   separate (Figure 7a), and after centrifugation, RGO remains mostly in the top surfactant phase

351   (Figure 7b). Similarly, when done in a wastewater matrix (i.e., 1 g biomass/L), the undigested

352   (interfering) biomass transfers into the water phase, and the RGO remains in the surfactant phase

353   (Figure 7c). This results in a physical separation of the RGO and the interfering background

354   carbon, allowing for easy recovery of the RGO only. Note, control samples digested with

355   Solvable for 36 hrs (i.e., no $NaBH_4$) did not show any significant (<5%) additional removal of

356   biomass interference. Therefore, using $NaBH_4$ to separate the biomass and RGO into different

357   phases is key for improving recovery in wastewater with a high biomass concentration. Using the

358   phase-separation method, the recovery of RGO (20µg) from 5 mg biomass was $110\% \pm 13\%$.

359   Recovery greater than 100% is attributed to undigested biomass constituents interacting with

360   RGO, causing the biomass to remain in the surfactant phase. This interaction is presumed to be

361   adsorption of the biomass to RGO as no interfering background carbon from the biomass was

362   observed in the surfactant phase for triplicate control samples that did not contain RGO. The

363   phase-separation was not successful for FLG as the majority of the FLG transferred to the water

364   phase along with the undigested biomass. The advantage of using the phase-separation method

16

365 over the centrifugal separation method for GO is that larger amounts of biomass can be used

366 while avoiding interferences from undigested biomass. However, in other instances, the

367 centrifugal method is preferred because it is simpler, less time consuming, and useful for both

368 graphene types. A detailed schematic of the two methods is shown in Figure SI-7.

369

370 **Conclusion**

371 We have successfully demonstrated an extraction and quantification method for graphene

372 and GO using an *in-situ* reduction method followed by detection with PTA. This method was

373 demonstrated in biomass (200 mg/L), resulting in recoveries for GO/RGO and FLG of $80 \pm 9\%$

374 and $52 \pm 8\%$, respectively. A phase-separation method (similar to liquid-liquid extraction) was

375 developed to improve the recovery of GO from more concentrated wastewater samples (e.g., 1 g

376 biomass/L). Although the phase-separation method is more complex than the centrifugal

377 separation method, it is an intriguing technique that warrants further investigation for highly

378 complex matrices (e.g., sediments). While FLG was easier to separate thermally using PTA, it

379 was more difficult to physically recover using the extraction method. This was for a specific type

380 of FLG, whereas other types from different manufacturers could behave differently. Further

381 study is needed on FLG and single-layer graphene to determine if physical recovery differences

382 exist between the varying types and if an additional processing step can improve the recovery.

383 Reported recoveries are ideal as they were obtained using a lab-grown, clean biomass.

384 When using biosolids obtained from a wastewater treatment plant, the recovery values are

385 expected to increase due to presence of soot particulates, which behave thermally similar to

386 graphene, thereby creating a false positive.[7] Similarly, the presence of carbonaceous

387 nanomaterials (e.g., CNTs, fullerenes) in environmental samples with graphene is possible,[33]

17

388   further complicating recovery when using PTA. While GO/RGO and FLG used herein can be

389   separated and quantified using PTA (e.g., Figure SI-7), the presence of CNTs with a similar

390   thermal stability as GO or FLG would be difficult to distinguish with PTA alone. Ideally, a

391   graphene standard (similar to the NIST single-walled CNT standard reference material, SRM

392   2483) would be used to create a spike standard addition curve in order to quantify the amount of

393   background soot (or CNTs) interfering with graphene. With the challenge of thermally similar

394   carbonaceous materials present (e.g., soot) or predicted (e.g., CNT) in the environment, PTA and

395   similar thermal methods alone are not currently suitable, and analytical advancements to these

396   methods and more selective extraction methods are needed. However, PTA, in its early analytical

397   development as described herein, is an excellent tool for monitoring the fate/transport and

398   toxicity of graphene for model systems and organisms, respectively.

399

407

408   **Supporting Information**

409   Additional figures.

410

References

1.   X. Q. Guo and N. Mei, *Journal of Food and Drug Analysis*, 2014, **22**, 105-115.
2.   A. B. Seabra, A. J. Paula, R. de Lima, O. L. Alves and N. Duran, *Chemical Research in Toxicology*, 2014, **27**, 159-168.
3.   G. X. Wang, J. Yang, J. Park, X. L. Gou, B. Wang, H. Liu and J. Yao, *Journal of Physical Chemistry C*, 2008, **112**, 8192-8195.
4.   M. S. Dresselhaus, A. Jorio and R. Saito, in *Annual Review of Condensed Matter Physics, Vol 1*, Annual Reviews, Palo Alto, 2010, pp. 89-108.
5.   D. A. Dikin, S. Stankovich, E. J. Zimney, R. D. Piner, G. H. B. Dommett, G. Evmenenko, S. T. Nguyen and R. S. Ruoff, *Nature*, 2007, **448**, 457-460.
6.   D. Li, M. B. Muller, S. Gilje, R. B. Kaner and G. G. Wallace, *Nature Nanotechnology*, 2008, **3**, 101-105.
7.   K. Doudrick, P. Herckes and P. Westerhoff, *Environmental Science and Technology*, 2012, **46**, 12246-12253.
8.   K. Doudrick, N. Corson, G. Oberdörster, A. C. Eder, P. Herckes, R. U. Halden and P. Westerhoff, *ACS Nano*, 2013, **7**, 8849-8856.
9.   D. L. Plata, C. M. Reddy and P. M. Gschwend, *Environmental Science & Technology*, 2012, **46**, 12254-12261.
10.   R. H. Wang, C. Mikoryak, E. Chen, S. Li, P. Pantano and R. K. Draper, *Analytical Chemistry*, 2009, **81**, 2944-2952.
11.   M. J. O'Connell, S. M. Bachilo, C. B. Huffman, V. C. Moore, M. S. Strano, E. H. Haroz, K. L. Rialon, P. J. Boul, W. H. Noon, C. Kittrell, J. P. Ma, R. H. Hauge, R. B. Weisman and R. E. Smalley, *Science*, 2002, **297**, 593-596.
12.   E. J. Petersen, Q. G. Huang and W. J. Weber, *Environmental Science & Technology*, 2008, **42**, 3090-3095.
13.   F. Irin, B. Shrestha, J. E. Canas, M. A. Saed and M. J. Green, *Carbon*, 2012, **50**, 4441-4449.
14.   S. Attal, R. Thiruvengadathan and O. Regev, *Analytical Chemistry*, 2006, **78**, 8098-8104.
15.   R. B. Reed, D. G. Goodwin, K. L. Marsh, S. S. Capracotta, C. P. Higgins, D. H. Fairbrother and J. F. Ranville, *Environmental Science-Processes & Impacts*, 2013, **15**, 204-213.
16.   J. F. Shen, Y. Z. Hu, M. Shi, X. Lu, C. Qin, C. Li and M. X. Ye, *Chemistry of Materials*, 2009, **21**, 3514-3520.
17.   S. Gilje, S. Han, M. Wang, K. L. Wang and R. B. Kaner, *Nano Letters*, 2007, **7**, 3394-3398.
18.   S. Dubin, S. Gilje, K. Wang, V. C. Tung, K. Cha, A. S. Hall, J. Farrar, R. Varshneya, Y. Yang and R. B. Kaner, *Acs Nano*, 2010, **4**, 3845-3852.
19.   D. C. Luo, G. X. Zhang, J. F. Liu and X. M. Sun, *Journal of Physical Chemistry C*, 2011, **115**, 11327-11335.
20.   R. Muszynski, B. Seger and P. V. Kamat, *Journal of Physical Chemistry C*, 2008, **112**, 5263-5266.
21.   Y. Si and E. T. Samulski, *Nano Letters*, 2008, **8**, 1679-1682.

453   22.   W. Gao, L. B. Alemany, L. J. Ci and P. M. Ajayan, *Nature Chemistry*, 2009, **1**, 403-408.
454   23.   H. J. Shin, K. K. Kim, A. Benayad, S. M. Yoon, H. K. Park, I. S. Jung, M. H. Jin, H. K.
455   Jeong, J. M. Kim, J. Y. Choi and Y. H. Lee, *Advanced Functional Materials*, 2009, **19**,
456   1987-1992.
457   24.   B. Nowack, J. F. Ranville, S. Diamond, J. A. Gallego-Urrea, C. Metcalfe, J. Rose, N.
458   Horne, A. A. Koelmans and S. J. Klaine, *Environmental Toxicology and Chemistry*,
459   2012, **31**, 50-59.
460   25.   P. K. Westerhoff, A. Kiser and K. Hristovski, *Environmental Engineering Science*, 2013,
461   **30**, 109-117.
462   26.   I. Chowdhury, M. C. Duch, N. D. Mansukhani, M. C. Hersam and D. Bouchard,
463   *Environmental Science & Technology*, 2013, **47**, 6288-6296.
464   27.   Y. F. Wang, P. Westerhoff and K. D. Hristovski, *Journal of Hazardous Materials*, 2012,
465   **201**, 16-22.
466   28.   T. Y. Sun, F. Gottschalk, K. Hungerbuhler and B. Nowack, *Environmental Pollution*,
467   2014, **185**, 69-76.
468   29.   USEPA, in *Part 136 Guidelines Establishing Test Procedures for the Analysis of
469   Pollutants: Definition and Procedure for the Determination of the Method Detection
470   Limit*, USEPA, 2012.
471   30.   S. Osswald, M. Havel and Y. Gogotsi, *Journal of Raman Spectroscopy*, 2007, **38**, 728-
472   736.
473   31.   B. Scheibe, E. Borowiak-Palen and R. J. Kalenczuk, *Materials Characterization*, 2010,
474   **61**, 185-191.
475   32.   J. F. Liu, J. B. Chao, R. Liu, Z. Q. Tan, Y. G. Yin, Y. Wu and G. B. Jiang, *Analytical
476   Chemistry*, 2009, **81**, 6496-6502.
477   33.   F. Gottschalk, T. Y. Sun and B. Nowack, *Environmental Pollution*, 2013, **181**, 287-300.

478

20
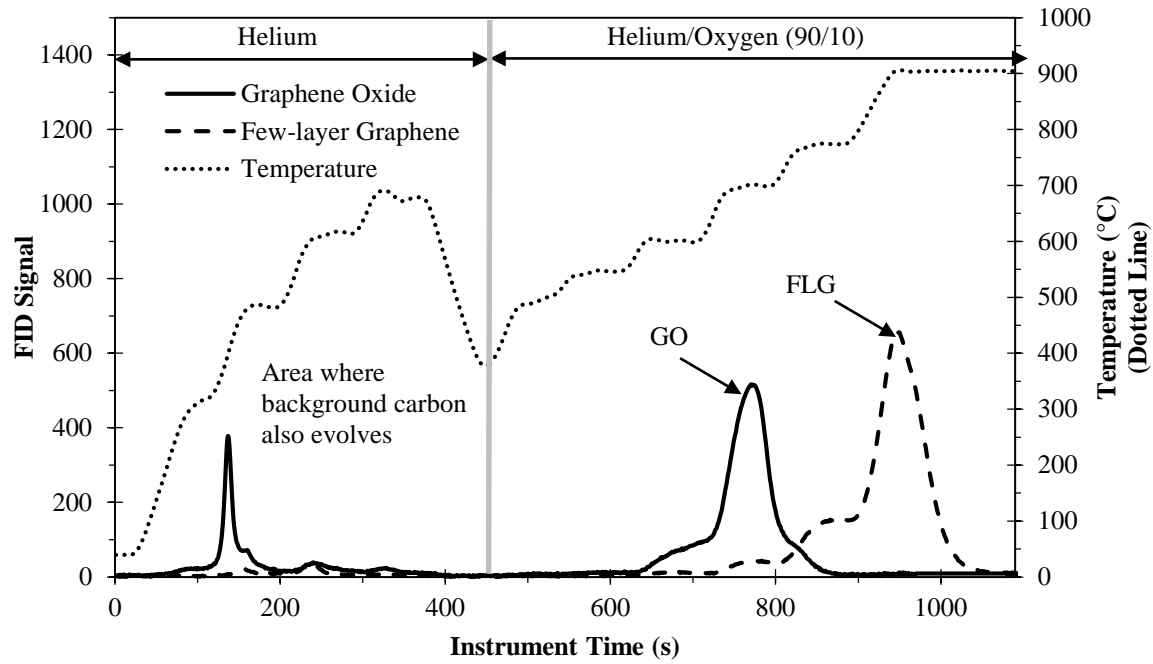
2   Figure 1. PTA thermograms for few-layer graphene (FLG) and graphene oxide (GO).

1

1
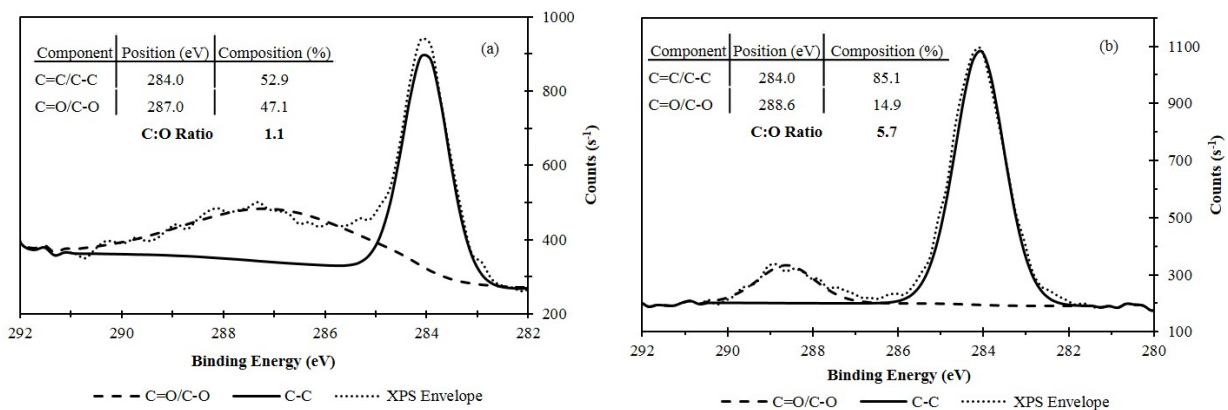
Figure 2. XPS analysis of (a) GO and (b) RGO. The average position for C=C and C-C was

284.0 eV, and the average position for C=O and C-O was 287.0 eV and 288.6 eV for GO and

RGO, respectively.
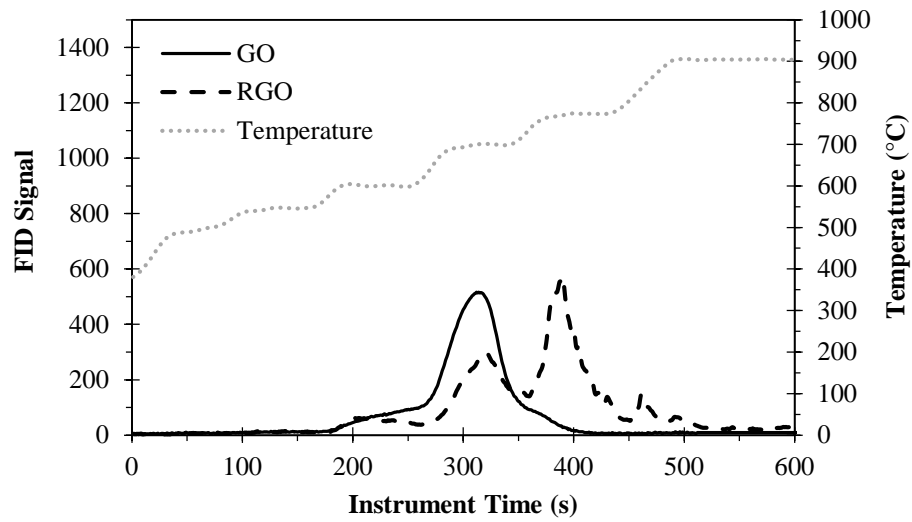
1

2   Figure 3. PTA thermograms (oxidizing phase) for RGO reduced with 2% NaBH$_4$ in water.

1
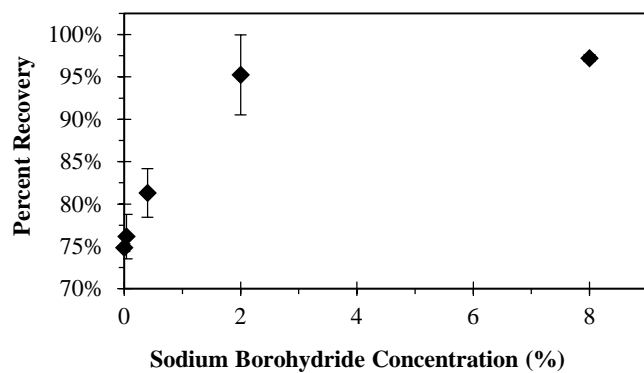
1

2   Figure 4. Percent recovery of RGO after GO reduction using various concentration of NaBH$_4$ (0,

3   0.04, 0.4, 2, 8%). Error bars indicate one standard deviation (each direction) for triplicate

4   samples.
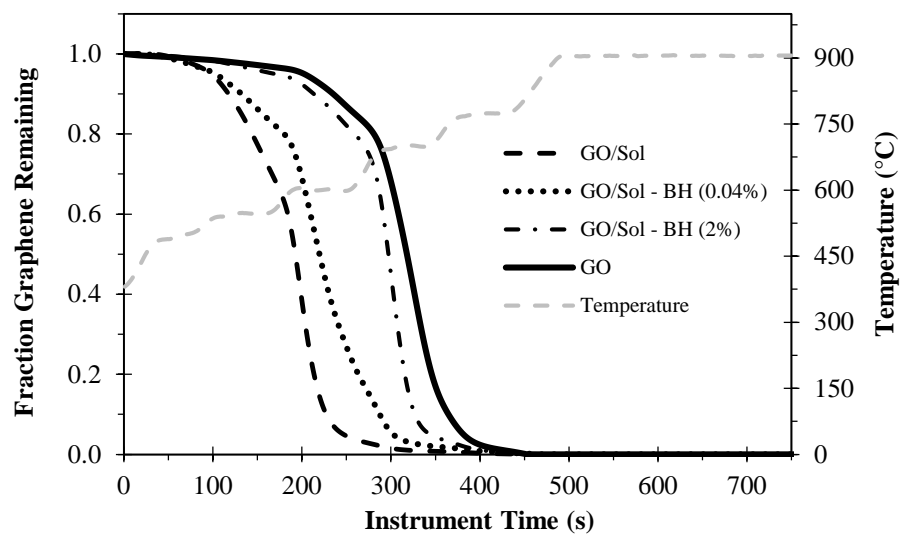
1

2   Figure 5. Mass loss curves for GO (~20 μg) under oxidizing PTA conditions using different

3   extraction conditions. "Sol" is Solvable and "BH" is NaBH$_4$.
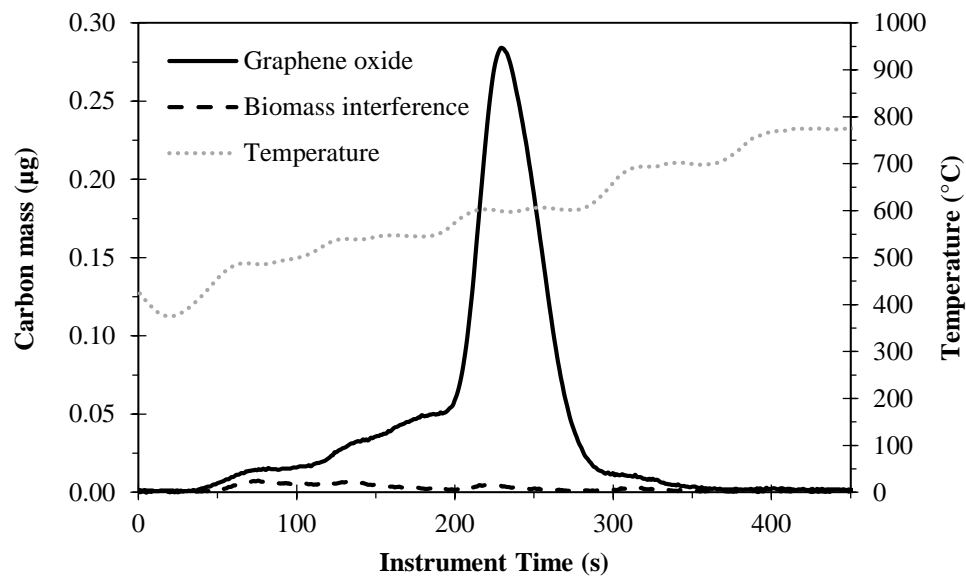
1

2   Figure 6. PTA thermogram showing biomass interference for GO in wastewater biosolids.

3   Solvable and 2% NaBH$_4$ treatment.
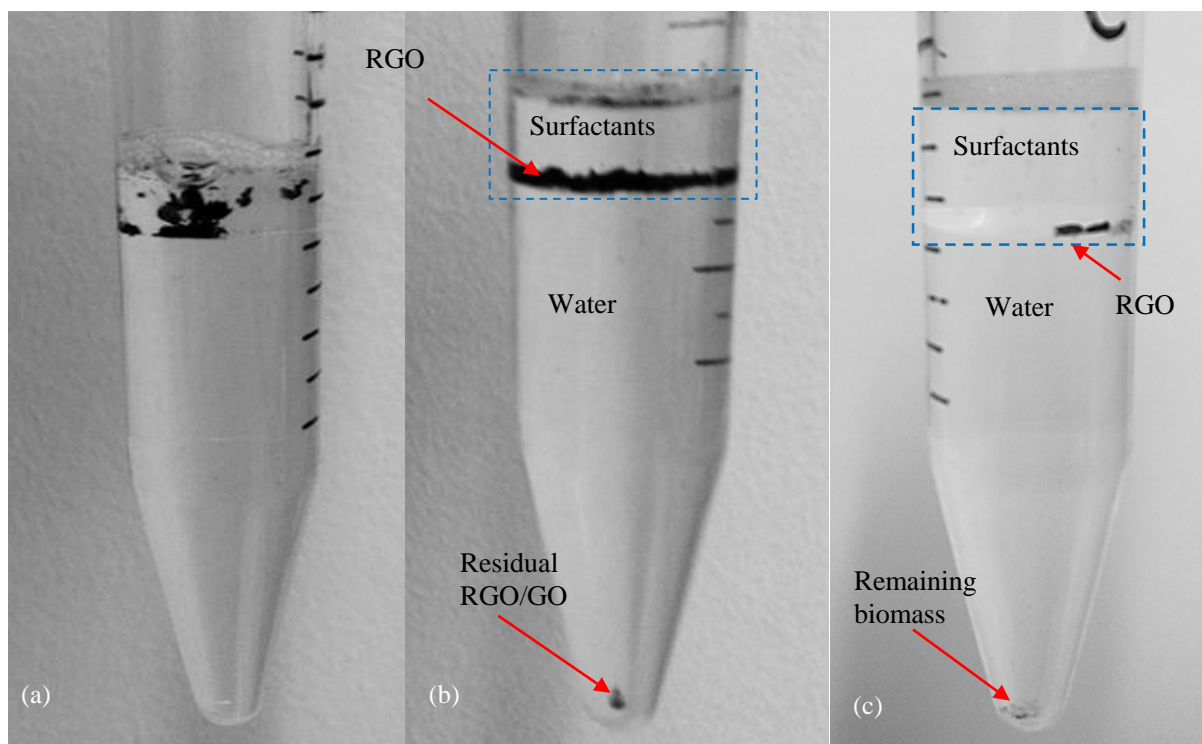
1

2   Figure 7. Images showing separation of water and surfactants with extended NaBH$_4$ treatment:

3   (a) RGO before centrifugation control sample, (b) RGO after centrifugation control sample, and

4   (c) RGO after centrifugation in 5 mg biomass sample. RGO is trapped in the surfactant phase,

5   and GO and undigested biomass are centrifuged down into the water phase.